

COMPLEX ATTOSECOND TRANSIENT-ABSORPTION SPECTROSCOPY

DISSERTATION

Presented in Partial Fulfillment of the Requirements for the Degree Doctor of
Philosophy in the Graduate School of The Ohio State University

By

Stephen J. Hageman, M.Sc.

Graduate Program in Physics

The Ohio State University

2019

Dissertation Committee:

Louis F. DiMauro, Advisor

Douglass Schumacher

Jay Gupta

Robert Baker

© Copyright by
Stephen J. Hageman
2019

ABSTRACT

The complex dipole is reconstructed in a transient absorption experiment.

Dedicated to coffee

ACKNOWLEDGMENTS

I would like to thank Sir Rickenabcker First of His Name, Last of His Kind, for his eternal indifference.

VITA

June 2011	Bachelors of Science in Physics and Mathematics, Johns Hopkins University
Dec 2014	Master of Science in Physics, The Ohio State University

Publications

“Rapid thermal annealing study of magnetoresistance and perpendicular anisotropy in magnetic tunnel junctions based on MgO and CoFeB”, Wei-Gang Wang, **Stephen Hageman**, *et al.*, Applied Physical Letters. I am a contributing author and performed many of the measurements of magnetoresistance. [Link to electronic version](#).

Table of Contents

	Page
Abstract	ii
Dedication	iii
Acknowledgments	iv
Vita	v
List of Figures	vii
List of Abbreviations	vii

Chapters

1 Two-source high harmonic generation	1
1.1 Introduction	1
1.2 Theory	1
1.2.1 Laser beam shaping using diffractive optics	1
1.2.2 Beam splitting phase grating	5
1.2.3 Imperfect phase grating	7
1.3 Two-source high harmonic generation	7
Appendix A Square-Wave Phase Grating	14
Bibliography	15

List of Figures

Figure	Page
1.1 Schematic demonstrating how to use a diffractive optical element to shape the beam profile at the focal plane. A collimated coherent beam is incident upon a diffractive optical element which shapes the phase of the incident beam, and then a lens is used as a transform element to Fourier transform the beam at the focal plane. The intensity profile at the focal plane can be controlled by altering the spatial dependence of the phase imparted upon the incident beam by the phase element. Adapted from [1]	2
1.2 Plot of the phase function $\phi(x - x_0)$ in units of π for a $0 - \pi$ square-wave phase grating (SWPG) with a period of d . The dark blue curve (light blue) shows the phase function for $x_0 = 0$ ($x_0 = d/10$).	6
1.3 Square complex modulus of the Fourier coefficients a_n of the $0 - \pi$ SWPG. The square complex modulus is proportional to the energy put into each diffraction order. As can be seen from figure, the ± 1 orders have the most energy put into them at $4/\pi^2 \approx 41.1\%$ each. All even orders have zero energy.	8
1.4 Intensity profile $S(\tilde{x})$ at the focal plane. Horizontal units are scaled by the spacing between orders, $\tilde{x}_1 = \lambda f/d$. Calculated by numerically propagation using Fresnel integral.	9
1.5 Intensity profile of the input beam measured by a thermal camera. Phase imparted by SWPG	10
1.6 (a) Two-channel model for Feshbach resonance. Incident atoms in the entrance channel (the open channel) couple to a bound state of energy E_c supported by the closed channel. Since collisions take place for $E \rightarrow 0$, tuning E_c to 0 allows for the resonant coupling to occur. (b) Scattering length near a resonance where a bound state crosses the scattering threshold. Inset shows the quadratic behavior of the binding energy near the resonance.	10
1.7 Camera image of two sources generating a filament in a gas cell. Image was taken while chamber was vented and at ambient pressure.	12
1.8 Camera image of the output of the phosphor screen. Harmonics are visible by eye.	13

Chapter 1

TWO-SOURCE HIGH HARMONIC GENERATION

1.1 Introduction

A common difficulty in working with extreme ultraviolet (XUV) light is the lack of efficient and broadband optics, especially beam splitters. In this chapter, I will introduce a method for generating two sources of XUV light by high harmonic generation using a **SWPG**. This **SWPG** allows for the duplication of an **infrared (IR)** pulse, as well as precise and stable control of the relative phase between the duplicates of the input **IR** pulse. The two most intense duplicates can generate harmonics which will interfere in the far-field. This can be thought of as an inline Mach-Zehnder interferometer with interferometric stability on sub-wavelength level of the high harmonic. The inherent stability of this two-source scheme will be utilized to measure both the real and imaginary parts of the refractive index of a medium.

1.2 Theory

1.2.1 Laser beam shaping using diffractive optics

In many experimental designs, it is advantageous to be able to shape the spatial intensity distribution of light to be something other than a typical Gaussian beam. A common example of this is generating a beam with an approximately constant intensity across its spatial profile (a flat-top beam). For the experiments described herein, we will be interested in duplicating an input beam with relative phase control between the two duplicate beams. Both of these examples are part of the general concept of laser beam shaping. The challenge is to design an optical system such that given an input beam profile $I_{in}(x, y)$ we can generate the desired output beam profile $I_{out}(x, y)$. Ideally, this optical system is designed in such

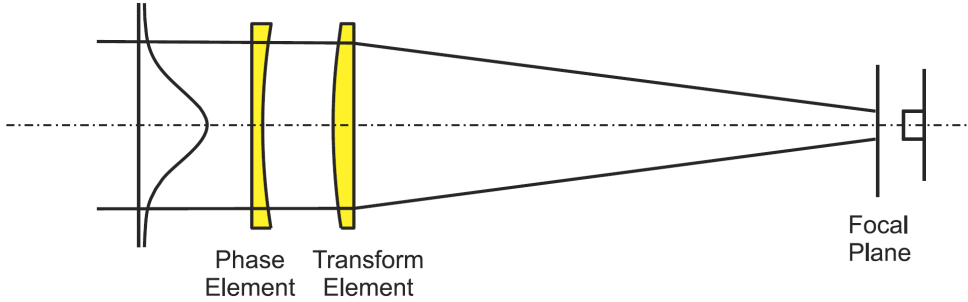


Figure 1.1: Schematic demonstrating how to use a diffractive optical element to shape the beam profile at the focal plane. A collimated coherent beam is incident upon a diffractive optical element which shapes the phase of the incident beam, and then a lens is used as a transform element to Fourier transform the beam at the focal plane. The intensity profile at the focal plane can be controlled by altering the spatial dependence of the phase imparted upon the incident beam by the phase element. Adapted from [1]

a way that it can be nearly lossless.¹ The relevant optical system which will be used is shown in figure 1.1. The system consists of a phase element which modifies the input field by $\phi(x, y)$ and a Fourier transform lens which adds a quadratic phase to the beam to focus it at the focal plane. By appropriate choice of the phase profile of the phase element, one can produce the desired beam profile at the focal plane.

This problem can be theoretically described in terms of Fourier optics [1–3]. If one assumes that a field $u(x, y, 0)$ is incident upon an aperture at $z = 0$, then the field for $z > 0$ can be written under the Fresnel approximation by the Fresnel integral

$$u(x, y, z) = \frac{ik}{2\pi z} e^{ikz} e^{ik(x^2+y^2)/2z} \int_{-\infty}^{\infty} \int_{-\infty}^{\infty} u(\xi, \eta, 0) e^{ik(\xi^2+\eta^2)/2z} e^{-ik(x\xi+y\eta)/z} d\xi d\eta \quad (1.1)$$

where $u(\xi, \eta, 0)$ is the incoming field and $k = 2\pi/\lambda$ is the wavenumber. Now, if one assumes that the phase element is placed at $z = 0$, then immediately after passing through the thin phase element in Fig. 1.1 the field is given by

$$u(\xi, \eta, 0) = f(\xi, \eta) e^{i\phi(\xi, \eta)}. \quad (1.2)$$

After propagating through the thin Fourier transform lens of focal length f , the field at the focal plane is now given by

$$u(x, y, f) = \frac{ik}{2\pi f} e^{ikf} e^{ik(x^2+y^2)/2f} \int_{-\infty}^{\infty} \int_{-\infty}^{\infty} f(\xi, \eta) e^{i\psi(\xi, \eta)} e^{-ik(x\xi+y\eta)/f} d\xi d\eta \quad (1.3)$$

¹In the limit of geometric optics it is possible to make the optical system, in principle, lossless, however this is not generally possible when one considers the wave nature of light.

where

$$\psi(\xi, \eta) = \phi(\xi, \eta) + k(\xi^2 + \eta^2)/2f. \quad (1.4)$$

Now, the idea is to rewrite this field profile at the focal plane into a more intuitive form by introducing the equation

$$g(\xi, \eta) = \frac{ik}{2\pi f} f(\xi, \eta) e^{i\psi(\xi, \eta)}. \quad (1.5)$$

The Fourier transform of this function $g(\xi, \eta)$ is given by

$$G(a, b) = \frac{ik}{2\pi f} \int_{-\infty}^{\infty} \int_{-\infty}^{\infty} f(\xi, \eta) e^{i\psi(\xi, \eta)} e^{-i(a\xi + b\eta)} d\xi d\eta. \quad (1.6)$$

By setting $a = kx/f$ and $b = ky/f$ and taking the square complex modulus, one obtains the equation

$$|G(kx/f, ky/f)|^2 = \frac{k^2}{(2\pi f)^2} \left| \int_{-\infty}^{\infty} \int_{-\infty}^{\infty} f(\xi, \eta) e^{i\psi(\xi, \eta)} e^{-ik(x\xi + y\eta)/f} d\xi d\eta \right|^2. \quad (1.7)$$

By comparing this equation with the square complex modulus of the field at the focal plane (equation 1.3), one finds the relationship

$$|u(x, y, f)|^2 = |G(kx/f, ky/f)|^2. \quad (1.8)$$

From this last equality we have shown that the intensity of the field at the focal plane $|u(z = f)|^2$, is given by the Fourier transform of the combined phase imparted upon the incident field by both the phase element and the Fourier transform lens, $|G|^2$. So, if one wants a specific beam shape $Q(x, y)$ at the focal plane, then by tuning the frequency components of the phase imparted upon the beam $\phi(x, y)$ and the focal length f used then one can achieve the desired beam profile, such that

$$|G(kx/f, ky/f)|^2 = Q(x, y). \quad (1.9)$$

This problem is difficult in general, so the challenge in many beam shaping problems is to try and minimize the error between the true field and the desired field, and to further complicate the matter, many applications will require different notions of error to be used. For example, if one needs the energy distribution to be as close as possible to the desired profile, then the ℓ_2 -norm would be appropriate. However, if the maximum intensity is of concern, then the ℓ_∞ -norm combined with the ℓ_2 -norm would be the appropriate notion of error.

It is possible to gain more insight into how difficult a beam shaping problem will be by reformulating the problem in terms of relevant length scales. The idea is to introduce a dimensionless parameter whose magnitude will reflect the validity of underlying assumptions,

and so for a given value of this parameter one can intuitively understand the performance (or lack thereof) of the beam shaping system. This is done by reformulating the above situation in terms of the natural length scales of both the incoming field and the desired field at the focal plane

$$I_{\text{input}} = |f(x, y)|^2 = |\hat{f}(x/\sigma, y/\sigma)|^2 \quad (1.10)$$

$$I_{\text{desired}} = Q(x, y) = \hat{Q}(x/d, y/d) \quad (1.11)$$

where σ is the characteristic length scale of the input field (typically the beam radius) and d is the characteristic length scale of the desired field. By expressing the fields in this way, we can now introduce the dimensionless parameter

$$\beta = \frac{2\pi\sigma d}{\lambda f}. \quad (1.12)$$

Using this dimensionless parameter, one can rewrite equations 1.6 and 1.9 as

$$G(\chi, \nu) = \int_{-\infty}^{\infty} \int_{-\infty}^{\infty} g(\xi, \eta) e^{-i(\chi\xi + \nu\eta)} e^{i\beta\hat{\psi}(\xi, \eta)} d\xi d\eta \quad (1.13)$$

$$|G(\chi, \nu)|^2 = \frac{4\pi^2 A}{\beta^2} Q(\chi/\beta, \nu/\beta) \quad (1.14)$$

where $\chi = x\sigma k/f$, $\nu = y\sigma k/f$, A is a constant, and $\hat{\psi} = \beta\psi$. From equation 1.2.1, it is clear that the functions g and G are related by a Fourier transform, so they must obey the uncertainty relation given by

$$\mu_g \mu_G \geq 1 \quad (1.15)$$

where μ is the second moment. Now, if one were to choose the phase profile of the phase element $\phi(x, y)$ such that equation 1.14 is satisfied, then one finds that $\mu_G = \beta^2 \mu_Q$. This then leads to the inequality

$$\beta^2 \mu_G \mu_Q \geq 1. \quad (1.16)$$

It can be seen that for large values of β this inequality can be readily satisfied. However, for very small values of β this inequality cannot be met and it will not be possible to produce the desired beam profile. From this, it can be seen that having a large value of β makes the beam shaping problem more tractable. The physical interpretation of β is that it is a measure of validity of geometric optics. It can be shown that when β is large a stationary phase method can be used to expand equation , and the lowest order term can be derived using a geometric optics approximation and higher order terms are related to the effects of diffraction [1, 2].

In this section, the general problem of laser beam shaping has been introduced and formulated as a problem in Fourier analysis, and by rewriting everything in terms of natural length scales we can infer which types of beam shaping problems will be more tractable using

geometrical optics approximations. The discussion so far has been kept very abstract, but in the next section the problem of interest will be introduced and these ideas will become more concrete.

1.2.2 Beam splitting phase grating

Now that the general theory behind laser beam shaping has been introduced, we move on to the specific problem at hand. The idea is to produce two nearly identical XUV beams through [high-harmonic generation \(HHG\)](#) using two nearly identical [IR](#) beams. The challenge is how to produce two nearly identical [IR](#) beams while minimizing the energy lost in the process. An additional requirement is that we can control the relative phase between these two [IR](#) beams. All of these requirements can be met through the use of a beam splitting phase grating.

As shown in section [1.2.1](#), the beam shape at the focal plane of a lens can be controlled through appropriate choice of a phase element and the spatially dependent phase $\phi(x, y)$ which is imparted upon the incoming beam. We will still consider the schematic shown in figure [1.1](#). However, the phase element which will be considered in this section (the beam splitting phase grating) will only modify the phase in one dimension, $\phi(x, y) = \phi(x)$, and it will be a periodic function with a period of d , $\phi(x) = \phi(x + d)$. If we expand the function $P(x) = e^{i\phi(x)}$ in a Fourier expansion

$$P(x) = \sum_{n=-\infty}^{\infty} a_n e^{\frac{i2\pi n x}{d}} \quad (1.17)$$

$$a_n = \frac{1}{d} \int_{-d/2}^{d/2} P(\tilde{x}) e^{-\frac{i2\pi n \tilde{x}}{d}} d\tilde{x}, \quad (1.18)$$

then it can be shown (see Appendix [A](#)) that each of the Fourier coefficients represents a diffracted beam and the energy contained in each diffracted beam is given by the square complex modulus of the Fourier coefficient $|a_n|^2$. Thus, by making our phase element in figure [1.1](#) a phase grating, we have split the beam into many diffraction orders. We have specified the period of the phase grating by requiring $\phi(x) = \phi(x + d)$, however we have not yet determined its shape. This can be accomplished by specifying the distribution of energy into the various diffraction orders. Since we want to split the incoming beam into two duplicate beams, we are searching for d -periodic function such that puts equal energy into two diffraction orders and a maximal amount of the input energy is put into those two orders. It can be shown (see Appendix [A](#)) that the d -periodic function which meets these criteria is a $0 - \pi$ [SWPG](#) given by

$$P(x, x_0) = \text{sign} \left(\cos \left(\frac{2\pi(x - x_0)}{d} \right) \right) \quad (1.19)$$

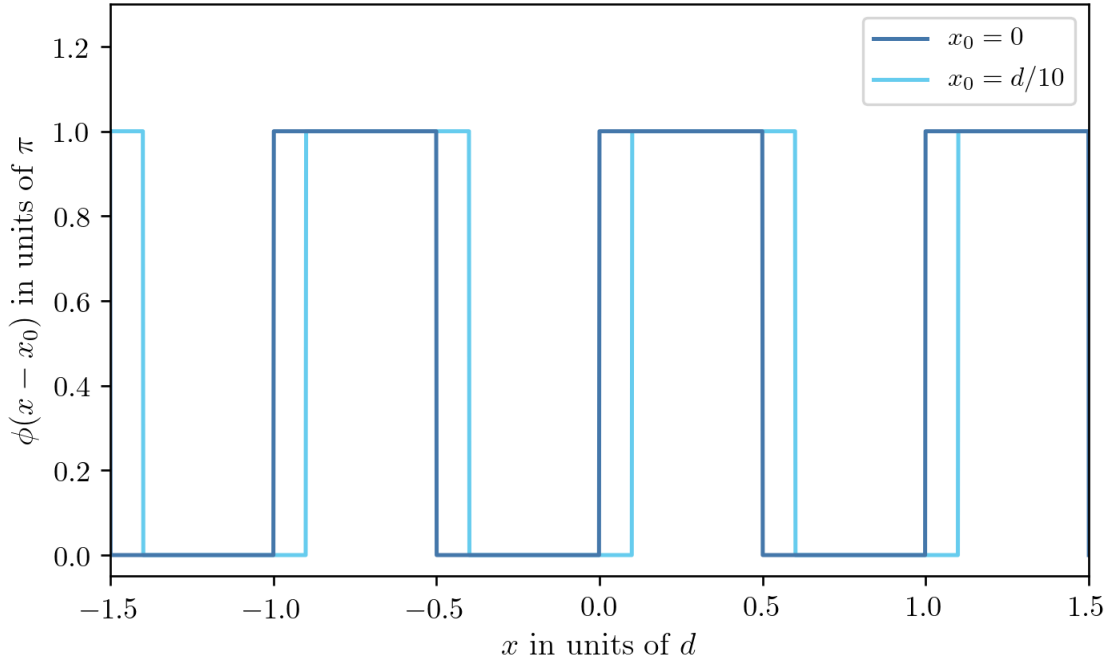


Figure 1.2: Plot of the phase function $\phi(x - x_0)$ in units of π for a $0 - \pi$ SWPG with a period of d . The dark blue curve (light blue) shows the phase function for $x_0 = 0$ ($x_0 = d/10$).

where x_0 is an offset of position of the **SWPG** in the plane transverse to the optical axis. From this equation, it can be seen that the phase of the incoming beam is modulated by either 0 or π , and this is shown in figure 1.2 for $x_0 = 0$ and $x_0 = d/10$.

From equation 1.17, we can calculate the Fourier coefficients $a_n(x_0)$ for the **SWPG** for $n = 0$ and $n \neq 0$. These Fourier coefficients determine how the energy is distributed between the different diffraction orders. For the zeroth-order case ($n = 0$), we find that

$$\begin{aligned} a_0(x_0) &= \frac{1}{d} \int_{-d/2}^{d/2} \text{sign} \left(\cos \left(\frac{2\pi(\tilde{x} - x_0)}{d} \right) \right) d\tilde{x} \\ a_0(x_0) &= \frac{1}{d} \left[- \int_{-\frac{d}{2}}^{-\frac{d}{4} + x_0} d\tilde{x} + \int_{-\frac{d}{4} + x_0}^{\frac{d}{4} + x_0} d\tilde{x} - \int_{\frac{d}{4} + x_0}^{\frac{d}{2}} d\tilde{x} \right] \\ a_0(x_0) &= 0. \end{aligned} \tag{1.20}$$

This demonstrates that zero energy is put into the zeroth-order diffraction for the $0 - \pi$

SWPG. For the other diffraction orders, we find that

$$\begin{aligned}
a_n(x_0) &= \frac{1}{d} \int_{-d/2}^{d/2} \text{sign} \left(\cos \left(\frac{2\pi(\tilde{x} - x_0)}{d} \right) \right) e^{-\frac{i2\pi n \tilde{x}}{d}} d\tilde{x} \\
&= \frac{1}{d} \left[- \int_{-\frac{d}{2}}^{-\frac{d}{4}+x_0} e^{-\frac{i2\pi n x}{d}} d\tilde{x} + \int_{-\frac{d}{4}+x_0}^{\frac{d}{4}+x_0} e^{-\frac{i2\pi n x}{d}} d\tilde{x} - \int_{\frac{d}{4}+x_0}^{\frac{d}{2}} e^{-\frac{i2\pi n x}{d}} d\tilde{x} \right] \\
&= \frac{1}{i2\pi n} \left[e^{\frac{i\pi n}{2} - \frac{i2\pi n x_0}{d}} - e^{in\pi} + e^{\frac{i\pi n}{2} - \frac{i2\pi n x_0}{d}} - e^{-\frac{i\pi n}{2} - \frac{i2\pi n x_0}{d}} + e^{-in\pi} - e^{-\frac{i\pi n}{2} - \frac{i2\pi n x_0}{d}} \right] \\
&= \frac{1}{i\pi n} \left[e^{\frac{i\pi n}{2} - \frac{i2\pi n x_0}{d}} - e^{-\frac{i\pi n}{2} - \frac{i2\pi n x_0}{d}} \right] = \frac{\sin(n\pi/2)}{n\pi/2} e^{-i\frac{2\pi n x_0}{d}} \\
a_n(x_0) &= \text{sinc}\left(\frac{n\pi}{2}\right) e^{-in\frac{2\pi x_0}{d}}.
\end{aligned} \tag{1.21}$$

Since $\text{sinc}(n\pi/2) = 0$ for even n , we see that only the odd orders of diffraction from the **SWPG** are populated. The distribution of energy between the different diffraction orders is plotted in figure 1.3, and from this figure it is immediately clear that our choice of the $0 - \pi$ **SWPG** has succeeded in putting most of the input energy equally into two diffraction orders, namely the ± 1 orders. The efficiency of this phase grating can be defined as

$$\eta = |a_1|^2 + |a_{-1}|^2 = \frac{8}{\pi^2} \approx 0.8106, \tag{1.22}$$

which means that approximately 81% of the input energy will be put into the two orders that we want. It should be noted that $\sum_n |a_n|^2 = 1$, which means that while we can't get perfect conversion of energy into two orders this is still a lossless design.

A very important feature of the **SWPG**

1.2.3 Imperfect phase grating

1.3 Two-source high harmonic generation

$$S(x) = \sum_n E(x - x_n) \tag{1.23}$$

$$\begin{aligned}
I_{IR} &= a + b \times \cos(\phi(x_0)) \\
I_q &= \alpha_q \times a^q \left(1 + N_q \frac{b}{a} \cos(\phi(x_0)) \right) + o(b \times a^{q-1})
\end{aligned} \tag{1.24}$$

$$\begin{aligned}
I_{IR}(\tilde{x}_1, x_0) &= \left| \tilde{S}(\tilde{x}_1, x_0) \right|^2 \\
&= \left| a_{-1} \tilde{E}(2\tilde{x}_1) + a_0 \tilde{E}(\tilde{x}_1) + a_1 \tilde{E}(0) + a_3 \tilde{E}(2\tilde{x}_1) \right|^2 \\
&= \left| a_0 \tilde{E}(\tilde{x}_1) + a_1 \tilde{E}(0) \right|^2
\end{aligned} \tag{1.25}$$

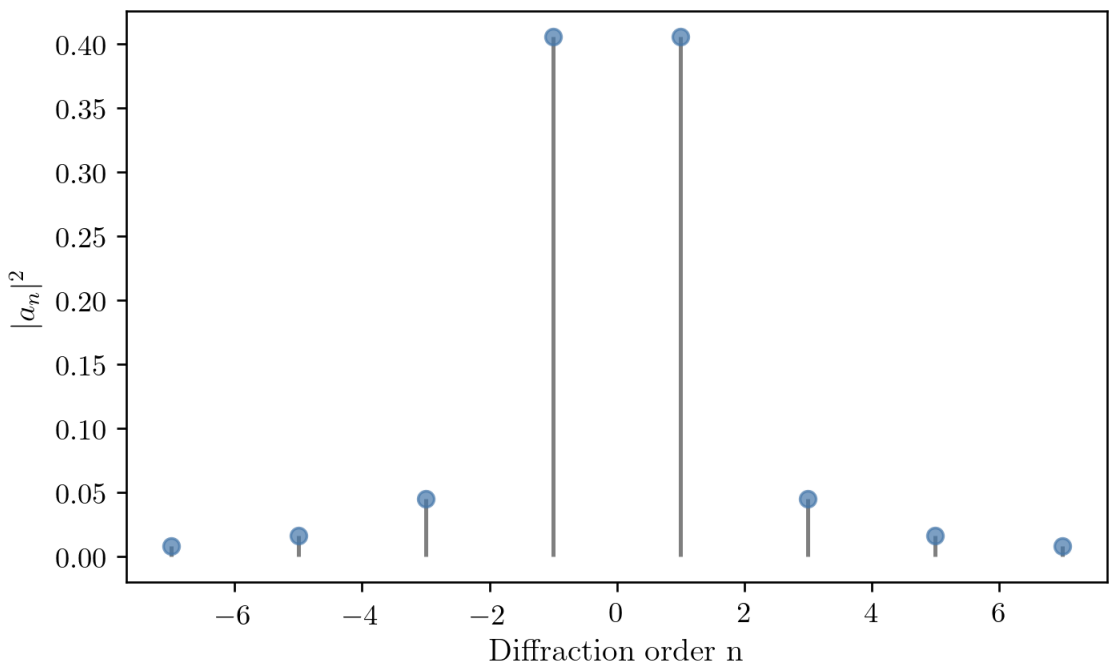


Figure 1.3: Square complex modulus of the Fourier coefficients a_n of the $0 - \pi$ SWPG. The square complex modulus is proportional to the energy put into each diffraction order. As can be seen from figure, the ± 1 orders have the most energy put into them at $4/\pi^2 \approx 41.1\%$ each. All even orders have zero energy.

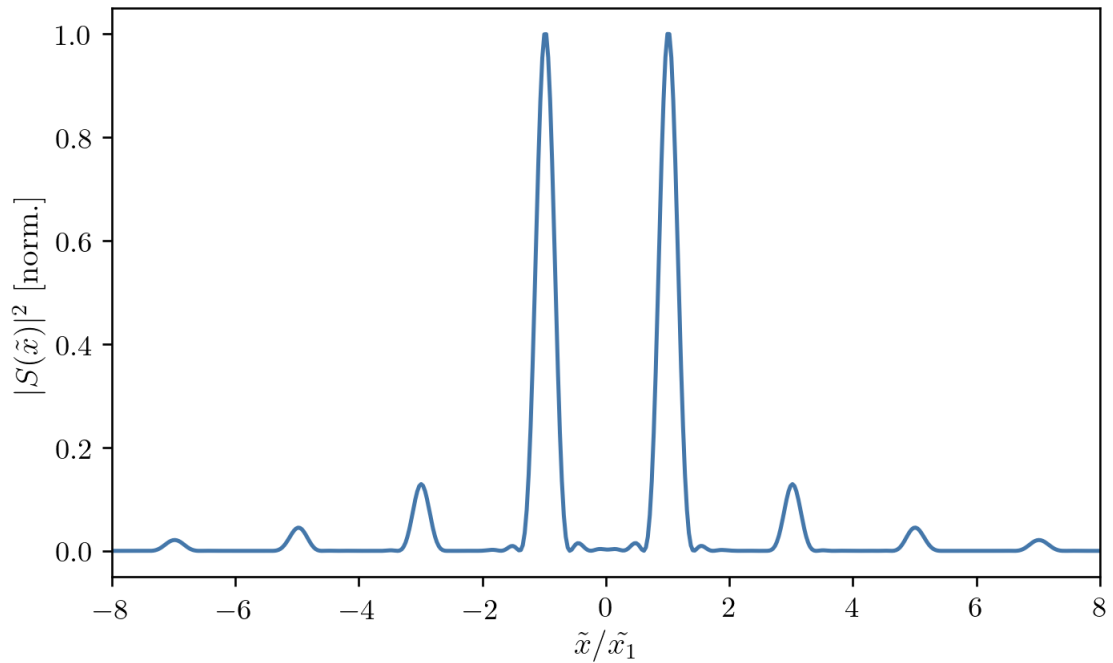


Figure 1.4: Intensity profile $S(\tilde{x})$ at the focal plane. Horizontal units are scaled by the spacing between orders, $\tilde{x}_1 = \lambda f/d$. Calculated by numerically propagation using Fresnel integral.

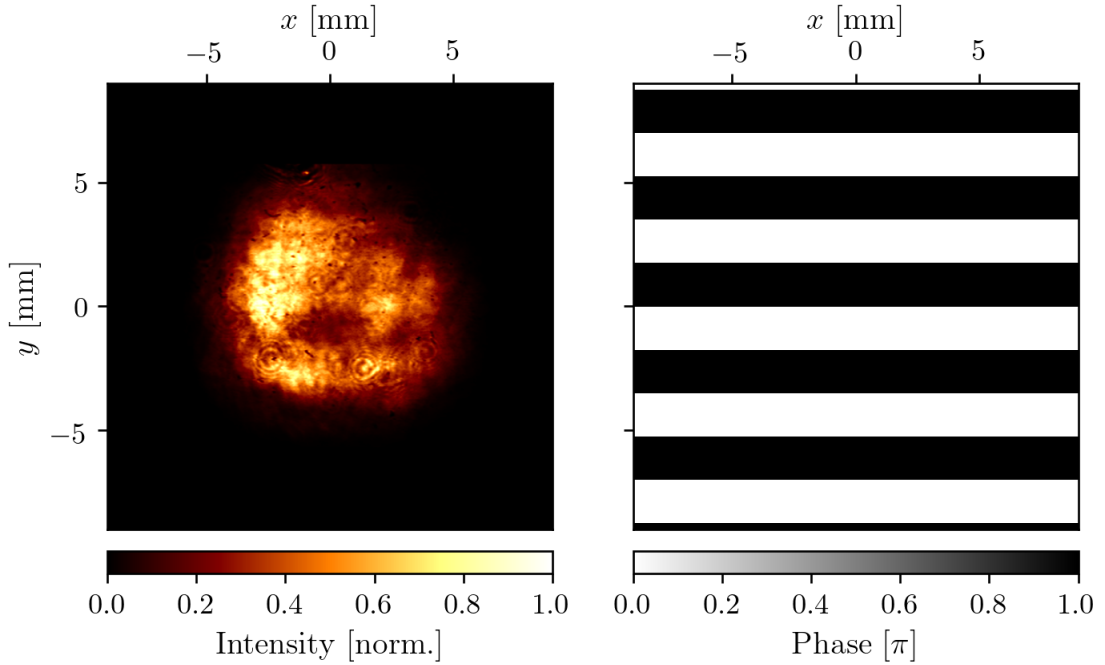


Figure 1.5: Intensity profile of the input beam measured by a thermal camera. Phase imparted by SWPG

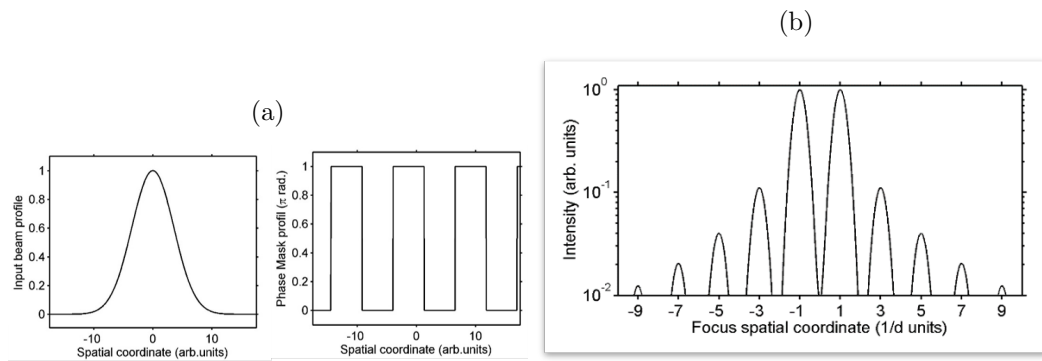


Figure 1.6: (a) Two-channel model for Feshbach resonance. Incident atoms in the entrance channel (the open channel) couple to a bound state of energy E_c supported by the closed channel. Since collisions take place for $E \rightarrow 0$, tuning E_c to 0 allows for the resonant coupling to occur. (b) Scattering length near a resonance where a bound state crosses the scattering threshold. Inset shows the quadratic behavior of the binding energy near the resonance.

$$I_{IR}(\tilde{x}_1, x_0) = \left| \tilde{E}(0) \right|^2 \left| \frac{2}{\pi} \sin\left(\xi \frac{\pi}{2}\right) e^{i(\xi \frac{\pi}{2} - \phi_1)} + \cos\left(\xi \frac{\pi}{2}\right) e^{i\xi \frac{\pi}{2}} \frac{\tilde{E}(\tilde{x}_1)}{\tilde{E}(0)} - \frac{2 \sin\left(\xi \frac{\pi}{2}\right)}{\pi} e^{i(\xi \frac{\pi}{2} + \phi_1)} \frac{\tilde{E}(2\tilde{x}_1)}{\tilde{E}(0)} + \frac{2 \sin\left(\xi \frac{\pi}{2}\right)}{3\pi} \right| \quad (1.26)$$

$$\begin{aligned} I_{IR}(\tilde{x}_1, x_0) &= \left| \tilde{E}(0) \frac{2}{\pi} \sin\left(\xi \frac{\pi}{2}\right) \right|^2 \left| e^{-i\phi_1} + \frac{\pi}{2 \tan\left(\xi \frac{\pi}{2}\right)} \frac{\tilde{E}(\tilde{x}_1)}{\tilde{E}(0)} - e^{i\phi_1} \frac{\tilde{E}(2\tilde{x}_1)}{\tilde{E}(0)} + \frac{e^{-3i\phi_1}}{3} \frac{\tilde{E}(2\tilde{x}_1)}{\tilde{E}(0)} \right|^2 \\ &= \left| \tilde{E}(0) \frac{2}{\pi} \sin\left(\xi \frac{\pi}{2}\right) \right|^2 \left(1 + \frac{\pi}{\tan\left(\xi \frac{\pi}{2}\right)} \frac{\tilde{E}(\tilde{x}_1)}{\tilde{E}(0)} \cos(\phi_1) - \frac{4}{3} \frac{\tilde{E}(2\tilde{x}_1)}{\tilde{E}(0)} \cos(2\phi_1) \right) \\ I_{IR}(\tilde{x}_{-1}, x_0) &= \left| \tilde{S}(\tilde{x}_{-1}, x_0) \right|^2 \\ &= \left| a_{-1} \tilde{E}(0) + a_0 \tilde{E}(\tilde{x}_1) \right|^2 \\ &= \left| \tilde{E}(0) \right|^2 \left| -\frac{2}{\pi} \sin\left(\xi \frac{\pi}{2}\right) e^{i(\xi \frac{\pi}{2} + \phi_1)} + \cos\left(\xi \frac{\pi}{2}\right) e^{i\xi \frac{\pi}{2}} \frac{\tilde{E}(\tilde{x}_1)}{\tilde{E}(0)} + \frac{2 \sin\left(\xi \frac{\pi}{2}\right)}{\pi} e^{i(\xi \frac{\pi}{2} - \phi_1)} \frac{\tilde{E}(2\tilde{x}_1)}{\tilde{E}(0)} - \frac{2 \sin\left(\xi \frac{\pi}{2}\right)}{3\pi} \right| \\ &= \left| \tilde{E}(0) \frac{2}{\pi} \sin\left(\xi \frac{\pi}{2}\right) \right|^2 \left| e^{-i\phi_1} - \frac{\pi}{2 \tan\left(\xi \frac{\pi}{2}\right)} \frac{\tilde{E}(\tilde{x}_1)}{\tilde{E}(0)} - e^{i\phi_1} \frac{\tilde{E}(2\tilde{x}_1)}{\tilde{E}(0)} + \frac{e^{-3i\phi_1}}{3} \frac{\tilde{E}(2\tilde{x}_1)}{\tilde{E}(0)} \right|^2 \\ &= \left| \tilde{E}(0) \frac{2}{\pi} \sin\left(\xi \frac{\pi}{2}\right) \right|^2 \left(1 - \frac{\pi}{\tan\left(\xi \frac{\pi}{2}\right)} \frac{\tilde{E}(\tilde{x}_1)}{\tilde{E}(0)} \cos(\phi_1) - \frac{4}{3} \frac{\tilde{E}(2\tilde{x}_1)}{\tilde{E}(0)} \cos(2\phi_1) \right) \\ a_0^\xi(x_0) &= \cos\left(\xi \frac{\pi}{2}\right) e^{i\xi \frac{\pi}{2}} \end{aligned} \quad (1.27)$$

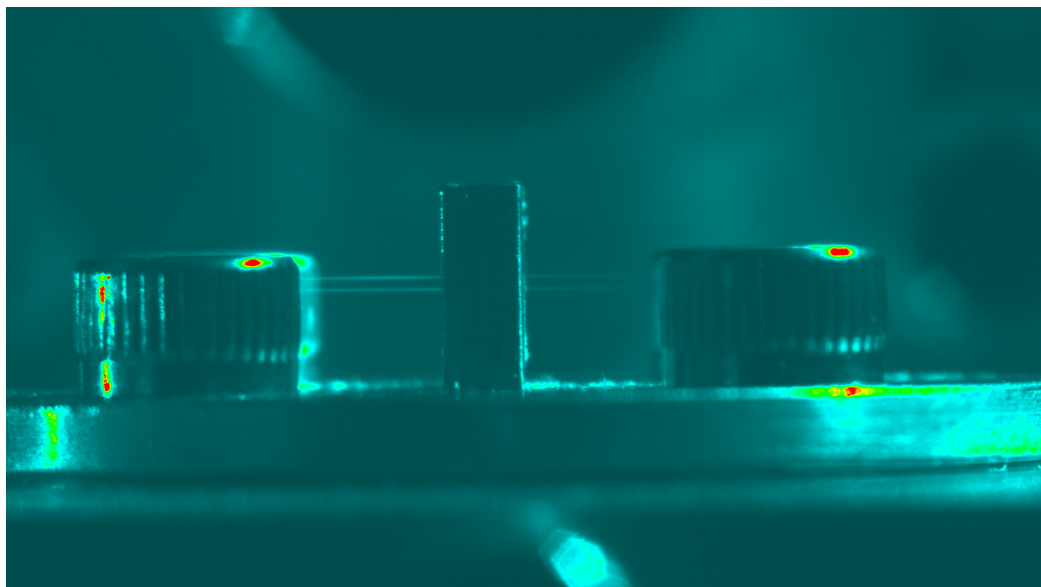


Figure 1.7: Camera image of two sources generating a filament in a gas cell. Image was taken while chamber was vented and at ambient pressure.

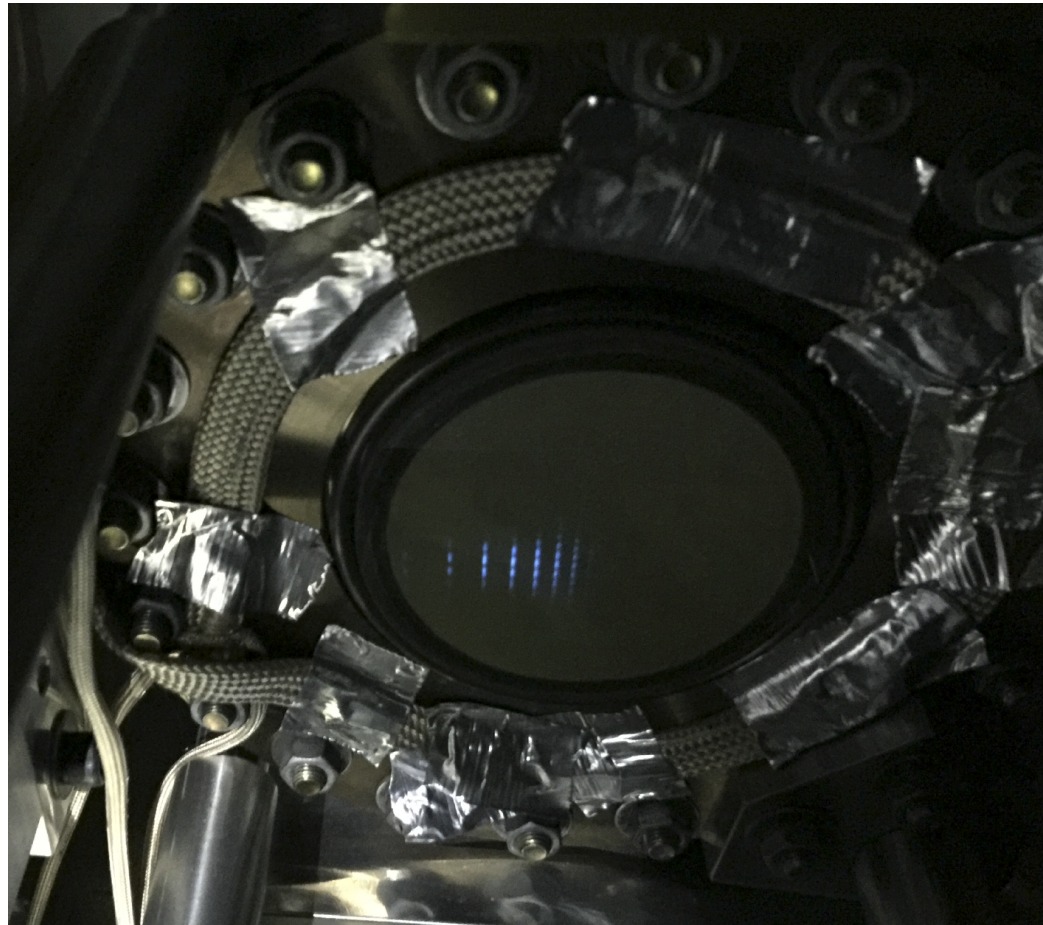


Figure 1.8: Camera image of the output of the phosphor screen. Harmonics are visible by eye.

Appendix A

SQUARE-WAVE PHASE GRATING

BIBLIOGRAPHY

- [1] L. A. Romero and F. M. Dickey. Mathematical aspects of laser beam shaping and splitting. page 765225.
- [2] Laser beam shaping: Theory and techniques.
- [3] Joseph W. Goodman. *Introduction to Fourier Optics*. Roberts & Co, 3rd ed edition. OCLC: ocm56632414.